Lakhe and Chaure, J Material Sci Eng 2015, 4:6
DOI: 10.4172/2169-0022.1000204

Journal of Material Sciences & Engineering

Research Article Open Access

Low-temperature Heat Treatment (80°C) Effect on the Electrochemically Synthesized $CuInTe_2$ Thin Films for Energy Harvesting Applications

Lakhe M and Chaure NB*

Electrochemical Laboratory, Department of Physics, Savitribai Phule Pune University, Pune, 411007, India

Abstract

We have investigated the effect of low-temperature (80ºC) post-deposition heat treatment onto $CuInTe_2$ (CIT) thin films prepared by one-step electrochemical technique. Aqueous precursor solution consisting ionic species of Cu, In and Te with pH 4.0 was used for the growth of CIT layers. The deposition potential was optimized using cyclic voltammetry. Conventional three-electrode geometry was used to electrodeposit CIT thin films onto CdS substrates. The structural, optical, morphological, compositional and transport properties were studied with the aid of XRD, Raman, HRTEM, UV-Visible, FESEM, EDAX, I-V and C-V measurements. As-deposited samples were amorphous in nature, however upon heat treatment highly crystalline CIT thin films with tetragonal crystal structure were exhibited. The values of energy band gap for the films deposited at -0.7 V and -0.8 V versus Ag/AgCl were estimated to be in the range 1.02 eV to 1.1 eV. Compact, uniform, void free and well adherent films were deposited at -0.7 V and -0.8 V. The samples were heat treated at 80ºC for 60 minutes therefore, visible changes in the surface morphology were not observed by SEM. Indium rich films were electrodeposited for -0.7 V and -0.8 V, however upon heat treatment stoichiometric layers were obtained. Schottky diodes are formed with Au metal contact in all cases. The solar cell investigated under illumination at 1.5 AM exhibits the short circuit current density (Jsc), 40.75 mA/cm^2; open circuit voltage (Voc), 255 mV; fill factor (FF), 41% and power conversion efficiency (η), 4.01%. This low-temperature heat treatment procedure could be advantageous for the fabrication of CIT solar cells onto flexible substrates.

Keywords: $CuInTe_2$; Electrodeposition; Energy harvesting; Thin films; Solar cells

Introduction

The ternary chalcopyrite semiconductors are technologically important group of semiconductors because of their photo-functionality. The broad range of optical band gap offered by these materials has led their emergence as technologically significant device materials in photovoltaic industry. Recently, researchers at Stuttgart's Centre for Solar Energy and Hydrogen Research Laboratory have reported highest efficiency 21.7% on CIGS material [1]. The material's growth and processing on different substrates showed major changes in the material properties because of the change in geometry/orientation of the substrate [2]. Therefore, it is important to investigate the material properties on different interfaces which lead the researchers to garner a fundamental understanding of materials as well as device perspective. The influence of growth parameters and subsequent post-deposition heat treatment are equally important to get the preferred material with device properties. Duchatelet [3] have reported 12.4% efficiency from electrodeposited CIGS with annealing at 500 – 550ºC under the flow of pure hydrogen and subsequently sulfurization at 550 – 600ºC. Kobayashi [4] have reported the growth of CIGS by molecular beam epitaxy technique with three stage procedure with substrate 540ºC. Mise and Nakada [5] have thoroughly studied the effect of substrate temperature and film thickness on properties of $CuIn_3Te_5$ thin films prepared by single step co-evaporation. The films deposited at 250ºC temperature measured cell efficiency 6.28%. Subsequently the same group reported 6.92% efficiency [6] in presence of MgF_2 antireflection coating (MgF_2).

$CuInTe_2$ thin films can be synthesized by vacuum as well as non-vacuum techniques. Numerous preparation techniques have been reported in the literature, viz, co-evaporation of Cu, In and Te by molecular beam epitaxy [5,6], Bridgeman method [7], thermal evaporation [8], flash evaporation [9], chemical vapor transport [10] and electrodeposition [11]. The synthesis of CIT nanoparticles [12] and quantum dots [13] are also reported. The highest efficiency 6.92% has been reported by molecular beam epitaxy [6] technique with $CuIn_3Te_5$ as absorber layer. The substrate temperature 250ºC was maintained during deposition for base pressure 4×10^{-6} Pascal. The reported efficiency is still low could be due to recombination via trap state in bulk $CuIn_3Te_5$, poor quality of the film near the substrate and band gap fluctuations because of the disorders. CIT films have also been prepared by Bridgeman methods at high temperature ~ 1100ºC [7]. The films deposited by thermal evaporation and graphite box annealing contain number of secondary phases of In_xTe_y and Cu_2Te [8]. The single phase polycrystalline and single crystalline films have been obtained by flash evaporation and chemical vapor transport, respectively. The band gap for single crystalline and polycrystalline CIT films can vary from ~ 0.91 eV to 1.00 eV [14,15]. Electrodeposition is one of the low-cost and very successful techniques used for the deposition of chalcopyrite and kesterite thin films for photovoltaic applications [14-22], however, limited literature is available on the synthesis of CIT by electrodeposition technique [11,20,23,24]. Furthermore, none of the group has developed the solar cell devices with the electrodeposited CIT. Some limitations of electrodeposition technique are still open to resolve, such as the requirement of conducting substrate and the growth of controlled stoichiometric thin film over large area. The difficulty in growth of stoichiometric film is with electrodeposition are still open for thinner layer probably due to the uneven distribution of current.

***Corresponding author:** Chaure NB, Electrochemical Laboratory, Department of Physics, Savitribai Phule Pune University, Pune, 411007, India, Tel: 91202569 2678, 2569 9072, 2569 1709; E-mail: n.chaure@physics.unipune.ac.in

Received October 04, 2015; **Accepted** November 08, 2015; **Published** November 18, 2015

Citation: Lakhe M, Chaure NB (2015) Low-temperature Heat Treatment (80ºC) Effect on the Electrochemically Synthesized $CuInTe_2$ Thin Films for Energy Harvesting Applications. J Material Sci Eng 4: 204. doi:10.4172/2169-0022.1000204

This issue can be resolved with some extent for thicker film of thickness 2 to 3 µm. Here, we report the electrodeposition conditions for CIT and the effect of low-temperature heat treatment was thoroughly investigated by various characterization techniques. Low processing temperature of solar cell demonstrates good device properties, which could be effectively used for the preparation of solar cells on flexible substrates [25].

Experimental Details

$CuInTe_2$ thin films were potentiostatically electrodeposited on CdS coated conducting glass substrates at 75ºC from aqueous bath for pH ~ 4. CdS films were deposited onto fluorine doped tin oxide (FTO) coated glass substrates by chemical bath deposition. The preparation and characterization of the thin films is reported elsewhere [26]. Potentiostat/galvanostat Model, Biologic SP 300 was employed to study the cyclic voltammetry (CV) experiment and the electrodeposition of CIT films. The detailed growth mechanism along with half-electrode reaction is reported in our previous work [25]. CIT films were electrodeposited for -0.7 V and -0.8 V verses Ag/AgCl reference electrode. Prior to heat treatment the samples were stored in laboratory atmosphere for overnight to remove the water contents. Subsequently, the samples were heat treated at 80ºC for an hour with heating rate 1ºC per minute and cooled down to room temperature naturally. The electrodeposition of the sample was performed several times (10 to 20 times) in the freshly prepared electrolyte in order to study the adherence of layer to the substrate and compactness. The heat treatment experiment at 80°C, was performed onto CIT layers as well as CdS/CIT hetero-structure sole cell device at least 10 different sample to study the repeatability and reproducibility of the results. Typical results obtained on CIT and CdS/CIT solar cells are reported. Structural, optical, morphological, compositional, electrical and optoelectronic properties were studied thoroughly. The heat treatment results were repeated more than 4/5 times and results were repeatable. X-ray diffractometer (Model Bruker D8 Advance, Germany) of Cu Kα radiation, with λ = 0.154 nm was used to study the structural properties. Invia Renishaw Raman Microscope coupled with Philips CCD camera was employed to study the Raman spectroscopy. The continuous wave laser of wavelength 785 nm was used as an excitation source. The HRTEM and diffraction pattern was examined using TEM, model TECHNAI G^2. Optical measurements were performed using JASCO, UV-VIS-NIR Spectrophotometer model V-670. Elemental composition was obtained by TEM instrument. High magnified topographical images were obtained using FESEM, Model HITACHI S4800. Thermal evaporation system was employed to make the metal contacts on CIT samples for electrical and optoelectronic measurements. Frequency response analyzer (FRA) facility available in above mentioned potentiostat was used to study the C-V measurements at frequency 100 KHz. The transport properties were studied by ECOPIA HMS-3000 model at constant magnetic field 0.54 T and probe current 10 mA. The surface of CIT layer was etched with NaCN solution (0.2%) for 90 seconds prior to metal contact. The dark and illuminated J-V measurements were performed using above potentiostat equipped with necessary software and probe system at light intensity 100 mW cm^{-2} (AM 1.5).

Results and Discussion

X-Ray Diffraction

XRD spectra recorded for the as-deposited and heat treated samples electrodeposited for potentials -0.7 V and -0.8 V is depicted in Figure 1. Upon heat treatment at 80ºC for an hour, the sample exhibited polycrystalline nature, whereas untreated samples were

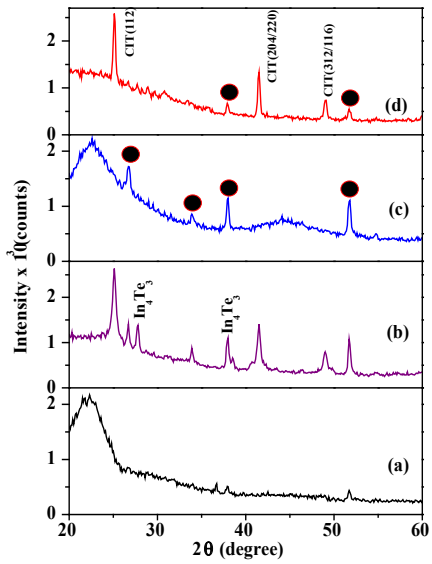

Figure 1: The XRD pattern of CIT samples deposited on CdS coated FTO substrate (a) and (c) as – prepared and (b) and (d) heat treated samples electrodeposited at -0.7 V and -0.8 V, respectively.

amorphous. The sharp XRD peaks attributed from heat treated samples at 2θ = 24.85º, 41.09º and 48.54º are corresponds to reflections (1 1 2), (2 0 4) / (2 2 0) and (3 1 2) / (1 1 6) respectively. CIT sample deposited at -0.8 V upon subsequent heat treatment exhibited the peak related to tetragonal structure of CIT along with the FTO (substrate) peaks, which are marked as solid circle (•). Additionally, secondary phases of In_4Te_3 along with CIT reflections were observed in the sample deposited at -0.7 V upon thermal heat treatment. The crystallinity for the CIT sample deposited at -0.8 V after heat treatment was found to be higher as compare to the sample deposited at -0.7 V after heat treatment. The average crystallite size is calculated by the Debey Scherrer equation [25]

$$D = \frac{0.9\lambda}{\Delta(2\theta)\cos\theta} \quad (1)$$

where D is the average crystallite size, λ is the X-ray wavelength (1.54056 Å), θ and Δ(2θ) are the Bragg diffraction angle of the XRD peak in degree and the full width at half maximum in radian, respectively. The average crystallite size 20 nm and 28 nm were determined for the heat treated samples deposited at – 0.7 V and - 0.8 V, respectively. The low-temperature heat treatment phenomenon related to enhancement in the crystallanity could be explained by lithification, diagenesis/catagenesis and metamorphism [27,28].

Raman Spectroscopy

Figures 2a and 2b depicts the Raman spectra of pristine and heat treated CIT samples electrodeposited for potentials -0.7 V and -0.8 V, respectively. The peaks observed in Raman spectra are in good agreement with the reported literature values [29]. In untreated samples, the broad hump from 100 cm^{-1} to 175 cm^{-1} is due to the mixing of 109 (B_2), 122 (A_1), 127(E), 141 (B_1), 159 (E) and 170 cm^{-1} (E and B_2) modes which is in good agreement with IR data [29]. The B_2 (109) mode is silent in the sample deposited at -0.7 V. Sharp peaks are observed upon annealing corresponds to A_1, B^3_1 and combination of E and B_2 modes. The related details are discussed elsewhere [25,29]. The spectra recorded for heat treated samples deposited at -0.7 V and -0.8

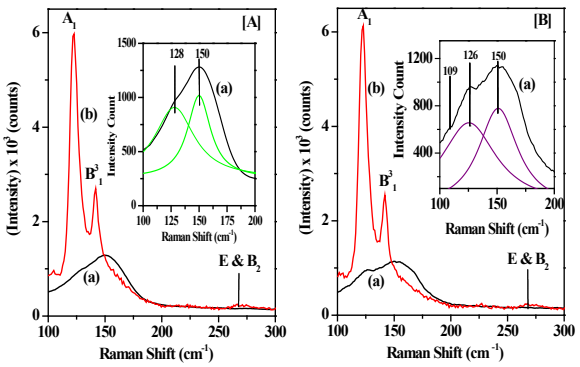

Figure 2: Raman Spectra of CIT samples deposited on CdS coated FTO substrate (a) as -prepared and (b) heat treated deposited at potential– 0.7 V [A] and – 0.8 V [B], respectively. Inset shows the Lorentzian fitting for as-deposited samples.

Mode	Standard Mode frequencies (cm^{-1})	Observed mode frequencies (cm^{-1})			
		-0.7 V		-0.8 V	
		Untreated	Heat treated	Untreated	Heat treated
E	109	silent	silent	109	silent
A_1	123	silent	123	silent	123
E	128	128	silent	126	silent
B^3_1	143	silent	142	silent	142
E	159	155	silent	155	silent
E^5 and/ or $B_2{}^3$	171	180	silent	silent	silent
E and B_2	267	261	267	silent	266

Table 1: Phonon mode frequencies of CIT samples on CdS coated FTO substrate compared with standard literature data.

V were very similar. The phonon modes attributed in the CIT samples and the literature values are summarized in Table 1.

Transmission Electron microscopy (TEM)

The high resolution transmission electron microscopy (HRTEM) and selected area diffraction pattern of the untreated and heat treated CIT films are shown in Figures 3a and 3b. The HRTEM images exhibits clear lattice fringes in heat treated samples (b) and (d) deposited at -0.7 V and -0.8 V, respectively. However the lattice fringes were not observed in the untreated samples. The interplaner distance 'd' measured for the samples deposited at -0.7 V and -0.8 V was found to be 0.19 nm and 0.36 nm which corresponds to the interplaner spacing of plane (316) and (112) of chalcopyrite CIT. The sharp continuous rings indicate the polycrystalline nature. These results agree well with structural results obtained by X-ray diffraction.

Optical properties

Figures 4a and 4b shows the plots of $(\alpha h\upsilon)^2$ verses energy ($h\upsilon$) of CIT thin films deposited at -0.7 and -0.8 V respectively. The data measured for untreated and heat treated sample is marked as (a) and (b) respectively. The energy band gap of untreated sample deposited at -0.7 V and -0.8 V was found to be ~ 1.05 eV and 1.07 eV respectively. However, upon heat treatment at 80ºC for an hour the values of bandgap was reduced to 0.9 eV to 1.0 eV due to the enhancement in particle size as well as the formation of polycrystalline CIT material. The estimated band gap values for untreated and heat treated CIT samples agreed well with the value reported by Mise [14].

Field Emission Scanning Electron Microscopy (FESEM)

The high magnified surface topographical images recorded for as prepared and heat treated sample is depicted in Figure 5. Compact and adherent thin films were deposited onto CdS substrate with almost uniform grain growth. The morphology of the sample upon thermal heat treatment was observed nearly similar as that of the untreated sample due to the low temperature (80ºC) heat treatment. Noticeable change was not expected in the morphology, however the improvement

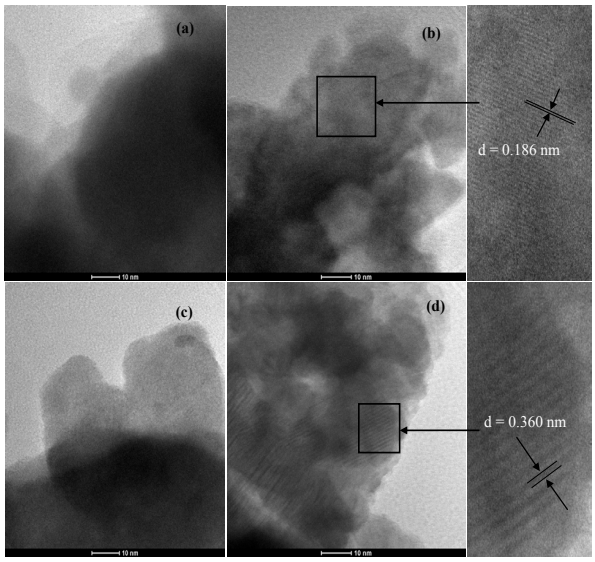

Figure 3a: HRTEM micrographs of CIT samples deposited on CdS coated FTO substrate (a) untreated (-0.7 V), (b) annealed (- 0.7 V), (c) untreated (-0.8 V) and (d) annealed (-0.8 V) A magnified region of annealed samples (b) and (d) shows fringing pattern.

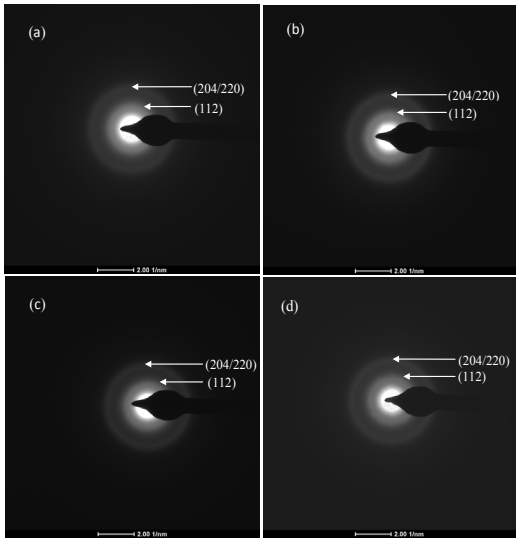

Figure 3b: Selected area diffraction pattern of CIT samples deposited on CdS coated FTO substrate (a) as - prepared (-0.7 V), (b) annealed (-0.7 V), (c) untreated (-0.8 V) and (d) annealed (-0.8 V).

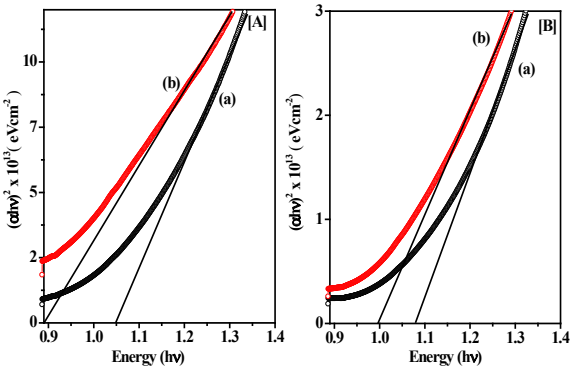

Figure 4: Plot of $(\alpha h\nu)^2$ verses Energy (hv) of CIT samples deposited on CdS coated FTO substrate (a) untreated and (b) annealed CIT samples deposited at – 0.7 V [A] and – 0.8 V [B].

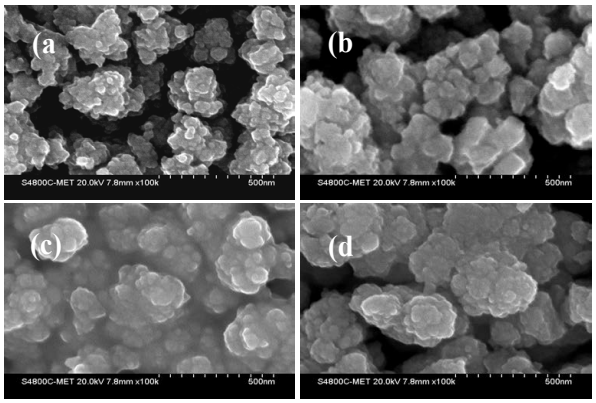

Figure 5: FESEM Images of FTO/CdS/CIT films (a) untreated (- 0.7 V), (b) annealed (- 0.7 V), (c) untreated (-0.8 V) and (d) annealed (- 0.8 V).

Deposition Potential (Volts)	Sample Condition	Elemental Composition in At. %			Cu/In ratio
		Cu	In	Te	
- 0.7	Untreated	19.57	23.05	57.38	0.85
	Heat treated	18.98	25.29	55.73	0.75
- 0.8	Untreated	17.81	29.56	52.62	0.60
	Heat treated	22.28	26.28	51.44	0.84

Table 2: A summary of elemental composition of CIT samples deposited on CdS substrate.

in the crystallinity noticed upon heat treatment is associated with an enhancement in compactness and reducing the grain boundaries with filling of Te and In_xTe_y related compound. Figures 5a and 5c are recorded for the untreated samples electrodeposited at -0.7 V and -0.8 V and their corresponding heat treated FESEM images are depicted in Figures 5b and 5d respectively.

A cauliflower like morphology with small visible voids can be clearly seen for the untreated CIT sample deposited at -0.7 V. The voids are due to the large cluster of size ~ 400-500 nm deposited on the surface. Upon heat treatment (Figure 5c) the voids were diminished and a good uniform surface with diffused grains can be seen. On the contrary, well adherent film was deposited at -0.8 V onto CdS substrates. The large clusters of size ~ 500 nm – 1000 nm was deposited at higher cathodic potential -0.8 V probably due to higher cathodic current.

Energy Dispersive Spectroscopy (EDS)

The elemental analysis was determined using the EDS assembly attached with TEM. A summary of the elemental atomic concentration in percentage obtained by EDS analysis is summarized in Table 2. The contents of Cu and Te were found to be more at -0.7 V as a counter part of sample deposited at -0.8 V. As the equilibrium potentials of Cu and Te are more positive than that of In, the deposition rate of Cu and Te was excepted more at low cathodic potentials. However, nearly stoichiometric CIT thin films were obtained upon the thermal heat treatment on the sample electrodeposited at -0.8 V. Upon heat treatment the Cu/In ratio for the sample deposited at -0.7 V was found to be decreased, whereas, the converse is true for the sample deposited for -0.8 V.

Hall measurement

Hall measurement set up with constant magnetic field 0.54 T and probe current 10 mA was employed to determine the electrical parameters hall-coefficient, bulk concentration, mobility, conductivity and resistivity. The average Hall-coefficient for all samples (untreated and heat treated) was positive, confirms the p-type conductivity. The carrier concentration calculated for all samples was of the order of 10^{19} cm^{-3}, which is slightly higher probably due to the higher concentration of Indium (In). As expected the conductivity 'σ' and mobility 'μ' were found to be increased upon heat treatment due to recrystallization of the material as well as the reduction of the grain boundaries. However, the mobility 'μ' is low as compare to other chalcopyrite materials [30], II-VI semiconductors [31] and silicon [32]. The values of the electrical parameters obtained by Hall measurement are tabulated in Table 3. Mobility values ~ 3 cm^2/Vs and 1.5 cm^2/Vs were reported for p-type $CuIn_3Te_5$ and $CuIn_5Te_8$ respectively by Wasim [33]. Prabhukanthan [10] has reported ~ 63 cm^2/Vs mobility for as-deposited and 105 cm^2/Vs for annealed CIT single crystal grown by chemical vapor transport. In the present data low mobility is due to the higher carrier concentration of the charge carriers. The mobility may be further improved with optimization of heat treatment conditions and surface treatment procedures.

Current density-Voltage (J-V) characteristics

The highly polycrystalline CIT thin films were obtained upon the heat treatment for the sample grown at -0.8 V verses Ag/AgCl reference, therefore we have prepared the solar cell for -0.8 V. Prior to metal contact the samples were etched in NaCN solution (0.2 wt%) for 90 seconds. A typical dark and illuminated photo current density - voltage (J-V) characteristics is shown in Figure 6. Illuminated curve is measured with 1.5 AM (100 mW cm^{-2}). The potential barrier, Φ_b was calculated under dark condition by the following equation [34];

$$\Phi_b = -\frac{kT}{q}\ln\left(\frac{A^{**}T^2}{J_s}\right) \quad (2)$$

where, 'Φ_b' is the barrier height, 'k' is the Boltzmann's constant, 'T' is the temperature, 'q' is the charge on electron, 'A^{**}' is the effective Richardson's constant for CIT material and 'J_s' is the reverse saturation current density. The barrier height 'Φ_b' was found to 0.49 eV. The solar cell exhibits the short circuit current density (Jsc), 40.75 mA/cm^2; open circuit voltage (Voc), 255 mV; fill factor (FF), 41% and power conversion efficiency (η), 4.01%. The low measured values of solar cell are due to the high Cu/In ratio, 0.84. The value of Cu/In ratio has to be around 0.26-0.30 [6,14] to prepare the high efficiency solar cells. Since the band gap of the CIT is in the IR region, the short circuit current

Deposition Potential (V)	Sample condition	Concentration (cm^{-3})	Mobility (cm^2/Vs)	Conductivity (1/Ω cm)	Resistivity (Ω cm)	Average Hall Coefficient cm^3/C
-0.7	Untreated	7.55×10^{19}	23.06	2.78×10^2	3.58×10^{-3}	8.27×10^{-2}
	Heat treated	6.48×10^{19}	29.44	3.05×10^2	3.27×10^{-3}	9.64×10^{-2}
-0.8	Untreated	8.36×10^{19}	18.40	2.46×10^2	4.05×10^{-3}	7.46×10^{-2}
	Heat treated	7.32×10^{19}	24.13	2.83×10^2	3.53×10^{-3}	8.52×10^{-2}

Table 3: Transport properties of the as-deposited and heat treated CIT samples.

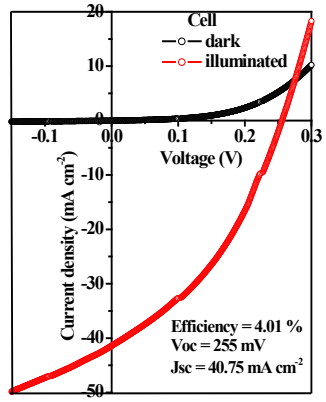

Figure 6: I-V characteristics measured for solar cell under dark and illuminated condition with light intensity 100 mW/cm² for FTO/CdS/CIT/Au.

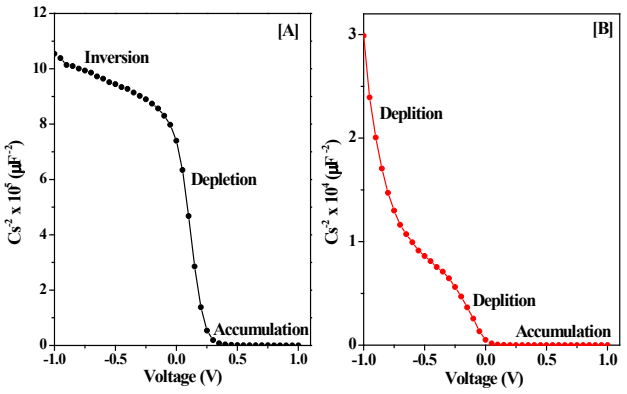

Figure 8: Plot $1/Cs^2$ verses Voltage (V) curve of a solar cell measured under A) dark and B) illuminated conditions.

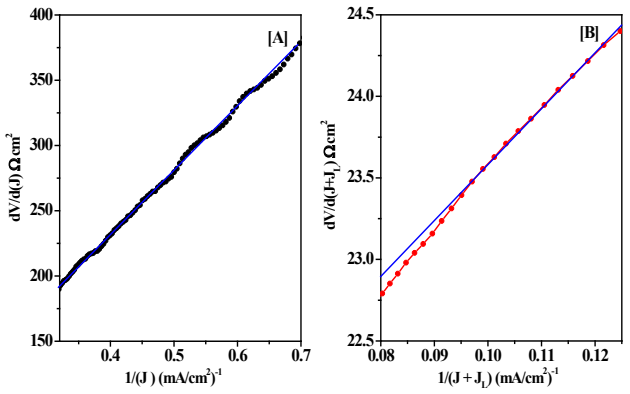

Figure 7: A typical plot of (a) dV/dJ versus (1/J) and (b) $dV/d(J + J_L)$ versus $1/(J + J_L)$ of solar cell device under dark and illuminated conditions, respectively.

density has almost close to the theoretical value but V_{oc} is found to low could be due to the recombination centers present in the space charge region. The series resistance "Rs' and ideality factor 'n' for cell under dark and illumination condition were deduced from the following diode equation [35];

$$J = J_o \, e \, xp \, [\frac{q}{n k_B T}(V - JR_s)] - J_L \qquad (3)$$

The intercept and slope of dV/dJ versus 1/(J) and $dV/d(J+JL)$ versus $\left(\frac{1}{J+JL}\right)$ depicted in Figure 7 give the values of series resistance, 'Rs' and ideality factor, 'n', respectively. The values of series resistance and ideality factor 193 Ω, 22.9 Ω and 4.84, 3.21 were obtained under dark and illuminated conditions, respectively. Both series resistance (Rs) and ideality factor (n) can be further reduced with optimization of heat treatment temperature, post –surface treatment and the duration of heating and etching of the sample.

Capacitance-Voltage measurement

The capacitance – voltage (Cs^{-2} versus V) measurement of the above solar cell was studied under dark and illuminated condition for frequency 100 kHz and shown in Figure 8. It is observed that the drift potential/flat band potential under dark is found to ~ 260 mV. Three regions i.e inversion, depletion and accumulation are clearly observed under dark condition. The carrier concentration under dark was calculated by following equation (4) [34] and found to be ~ 1.4 x 10^{19} cm^{-3} which agrees well with the charge carriers obtained from Hall Effect measurements.

$$N_A = \frac{2}{\varepsilon_s q}\left[-\frac{1}{\left(d\left(1/C^2\right)/dV\right)}\right] \qquad (4)$$

where 'N_A' is the acceptor concentration, 'q' is the charge on electron and 'ε_s' is the permittivity of semiconductor. The diffusion of charge carriers begins beyond 0.3 V under dark condition. Under illumination the clear inversion was not observed however, the device has found to be depleted two times showing the dominance of drift mechanism under reverse bias. A diffusion of charge carriers begins around 0.06 V shows the accumulation of charge carriers. It seems that device was found to be accumulated throughout the forward region indicates that forward current is due to the diffusion mechanism [6,36]. The carrier concentration under illumination is ~ 2.9×10^{21} cm^{-3}. The increase in charge carriers could be due to the generation of charge carriers under illumination.

Conclusion

Cathodic electrodeposition technique was successfully employed to deposit the $CuInTe_2$ thin films. Highly polycrystalline CIT films were obtained upon heat treatment at 80°C deposited for - 0.8 V. The most

prominent A_1 mode observed from the Raman spectra at 122 cm^{-1} in the heat treated samples confirms the formation of chalcopyrite structure. The HRTEM images exhibits clear lattice fringes upon heat treatment. The energy band gap of CIT samples was found to be ~ 1.05 eV and 1.07 eV for the deposited at -0.7 V and -0.8 V, respectively, which was reduced to 0.9 eV to 1.0 eV upon heat treatment. Compact, void free and well adherent layers with cauliflower like morphology of grain size ~ 500-1000 nm were deposited at -0.8 V. Cu/In ratio determined from EDS data was less than unity, which is suitable for high efficiency solar cells. The conductivity 'σ' and mobility 'μ' was found to be increased upon heat treatment due to re-crystallization and reduction in grain boundaries. P-type conductivity of CIT sample was confirmed with hall coefficient measurement. A typical solar cell investigated under illumination (1.5 AM) measured short circuit current density, (Jsc), 40.75 mA/cm^2; open circuit voltage (Voc), 255 mV; fill factor (FF), 41% and power conversion efficiency (η), 4.01%. This low-temperature heat treatment procedure could be advantageous for the fabrication of CIT solar cells onto flexible substrates. The device performance can be improved by controlling the concentration of depositing species, improving the heterojunction interface and changing the etching parameters.

Acknowledgement

The financial support received from University of Pune under DRDP, CNQS and DST PURSE is gratefully acknowledged. One of the authors ML would like to thank University Grant Commission (UGC) for UGC-BSR fellowship.

References

1. Jackson P, Hariskos D, Wuerz R, Kiowski O, Bauer A, et al. (2015) Properties of $Cu(In,Ga)Se_2$ solar cells with new record efficiencies up to 21.7%. Physica Status solidi (RRL) - Rapid Research Letter 9: 28-31.
2. Nelson N, Rakowski RT, Franks J, Woolliams P, Weaver P, et al. (2014) The effect of substrate geometry and surface orientation on the film structure of DLC deposited using PECVD. Surface & Coatings Technology 254: 73-78.
3. Duchatelet A, Sidali T, Loones N, Savidand G, Chassaing E, et al. (2013)12.4% Efficient $Cu(In,Ga)Se_2$ solar cell prepared from one step electrodeposited Cu-In-Ga oxide precursor layer. Solar Energy Materials & Solar Cells 119: 241-245.
4. Kobayashi T, Kumazawa T, Jehl Li Kao Z, Nakada T (2013) $Cu(In,Ga)Se_2$ thin film solar cells with a combined ALD-Zn(O,S) buffer and MOCVD-ZnO:B window layers. Solar Energy Materials & Solar Cells 119: 129-133.
5. Mise T, Nakada T (2011) Effects of substrate temperature and film thickness on properties of $CuIn_3Te_5$ thin films and solar cells. Journal of Applied Physics 110: 014504.
6. Mise T, Nakada T (2013) Narrow-bandgap $CuIn_3Te_5$ thin-film solar cells. Prog Photovolt Res Appl 21: 754-759.
7. Diaz R, Cervera M, Rueda F (2012) Impedance spectra and computation of chemical diffusion coefficients in $CuIn_3Te_5$ single crystals with a massive Cu motion. Journal of Physics D: Applied Physics 45: 235101 - 235110.
8. Roy S, Guha P, Chaudhuri S, Pal AK (2002) $CuInTe_2$ thin films synthesized by graphite box annealing of In/Cu/Te stacked elemental layers. Vacuum 65: 27-37.
9. Ananthan MR, Kasiviswanathan S (2009) Growth and characterization of stepwise flash evaporated $CuInTe_2$ thin films. Solar Energy Materials and Solar Cells 93: 188-192.
10. Prabukanthan P, Dhanasekaran R (2008) Growth of $CuInTe_2$ single crystals by iodine transport and their characterization. Materials Research Bulletin 43: 1996-2004.
11. Orts JL, Diaz R, Herrasti P, Rueda F, Fatas E (2007) $CuInTe_2$ and In-rich telluride chalcopyrites thin films obtained by electrodeposition techniques. Solar Energy Materials and Solar Cells 91: 621-628.
12. Kim C, Kim DH, Son YS, Kim H, Bae JY, et al. (2012) Solvothermal synthesis and characterization of a $CuInTe_2$ absorber for thin-film photovoltaics. Materials Research Bulletin 47: 4054-4058.
13. Kim S, Kang M, Kim S, Heo J, Noh JH, et al. (2013) Fabrication of $CuInTe_2$ and $CuInTe_{2-x}Se_x$ Ternary Gradient Quantum Dots and Their Application to Solar Cells. ACS Nano 6: 4756-4763.
14. Mise T, Nakada T (2010) Low temperature growth and properties of Cu-In-Te based thin films for narrow bandgap solar cells. Thin Solid Films 518: 5604-5609.
15. Ramanathan K, Teeter G, Keane JC, Noufi R (2005) Properties of high-efficiency $CuInGaSe_2$ thin film solar cells. Thin Solid Films 480-481: 499-502.
16. Chaure NB, Young J, Samantilleke AP, Dharmadasa IM (2004) Electrodeposition of p-i-n type $CuInSe_2$ multilayers for photovoltaic applications. Solar Energy Materials & Solar Cells 81: 125-133.
17. Bhattacharya RN (2013) CIGS-based solar cells prepared from electrodeposited stacked Cu/In/Ga layers. Solar Energy Materials & Solar Cells 113: 96-99.
18. Chaure NB, Samantilleke AP, Burton RP, Young J, Dharmadasa IM (2005) Electrodeposition of p^+, p, i, n and n^+ type copper indium gallium diselenide for development of multilayer thin film solar cells. Thin Solid Films 472: 212- 216.
19. Rohom AB, Londhe PU, Chaure NB (2015) The effect of pH and selenization on the properties of $CuInSe_2$ thin films prepared by electrodeposition technique for device applications. J Solid State Electrochem 19: 201-210.
20. Muftah GEA, Samantilleke AP, Warren PD, Heavens SN, Dharmadasa IM (2010) Electrochemical deposition of $CuInTe_2$ layers for applications in thin film solar cells. J Mater Sci Mater Electron 21: 373-379.
21. Londhe PU, Rohom AB, Chaure NB (2014) Selenization of electrodeposited copper-indium alloy thin films for solar cell applications. J Mater Sci Mater Electron 25: 4643-4649.
22. He X, Shen H, Wang W, Zhang B, Dai Y (2013) Quaternary co-electrodeposition of the Cu_2ZnSnS_4 films as potential solar cell absorbers. J Mater Sci Mater Electron 24: 572-575.
23. Dhanwate VN, Chaure NB (2013) Effect of growth potential on the electrodeposition of CIS thin films. Appl Nanosci 3: 1-5.
24. Pawar SM, Pawar BS, Moholkar AV, Choi DS, Yun JH, et al. (2010) Single step electrosynthesis of Cu_2ZnSnS_4 (CZTS) thin films for solar cell application. Electrochimica Acta 55: 4057-4061.
25. Lakhe M, Chaure NB (2014) Characterization of electrochemically deposited $CuInTe_2$ thin films for solar cell applications. Solar Energy Materials & Solar Cells 123: 122-129.
26. Chaure NB, Bordas S, Samantilleke AP, Chaure SN, Haigh J, et al. (2003) Investigation of electronic quality of chemical bath deposited cadmium sulphide layers used in thin film photovoltaic solar cells. Thin Solid Films 437: 10-17.
27. Miller D, Vandome AF, John AM (2010) Lithification, VDM Publishing (e - book).
28. Bucher K, Frey M (2002) Protogenesis of Metamorphic Rocks. Springer.
29. Rincon C, Wasim SM, Marin G, Huntzinger JR, Zwick A, et al. (1999) Raman spectra of the chalcopyrite compound $CuInTe_2$. Journal of Applied Physics 85: 3925.
30. Kodigala SR (2010) CIGS based thin film solar cells. 35.
31. Ray B (1969) II-VI Compounds. Rergamon Press Ltd, Oxford, London.
32. http://www.ioffe.rssi.ru/SVA/NSM/Semicond/Si/electric.html
33. Wasim SM, Rincon C, Marın G, Marquez R (2003) Electrical conduction in ordered defect compounds. Journal of Physics and Chemistry of Solids 64: 1627-1632.
34. Sze SM, Poplai HS (2006) Physics of Semiconductor Devices. Wiley Eastern Limited, New Delhi.
35. Chaure NB, Chaure S, Pandey RK (2004) Investigation of non-aqueous electrodeposited $CdS/Cd_{1-x}Zn_xTe$ heterojunction solar cells. Solar Energy Materials and Solar Cells 81: 39-60.
36. Hegedus SS, Shafarman WN (2004) Thin-Film Solar Cells: Device Measurements and Analysis. Prog Photovolt Res Appl 12: 155-176.